J|A|C|S
COMMUNICATIONS

Published on Web 10/30/2003

RNA Degradation in Cell Extracts: Real-Time Monitoring by Fluorescence Resonance Energy Transfer

Sarah A. Uhler, Dawen Cai, Yunfang Man, Carina Figge, and Nils G. Walter*
Department of Chemistry, University of Michigan, Ann Arbor, Michigan 48109-1055
Received June 23, 2003; E-mail: nwalter@umich.edu

The ability of an RNA molecule to persist in the cell among a plethora of ribonucleolytic activities is based on the tightly regulated relative rates of its synthesis and decay.[1] Regulation of specific mRNA turnover has long been studied, but the inability to derive rate constants with a convenient technique for directly monitoring RNA degradation has limited the introduction of predictive mathematical models.[2] In addition, the recent discovery of a multitude of short noncoding RNAs involved in gene regulation by RNA interference in eukaryotic genomes[3] and the advent of synthetic small interfering RNAs (siRNAs) for manipulating gene expression and probing gene function[4] have made an understanding of the rates and pathways of the cellular degradation of small RNA molecules indispensable.

Toward this goal, we have developed assays based on steady-state fluorescence resonance energy transfer (FRET) between two RNA-coupled fluorophores to observe nucleolytic decay of short synthetic RNAs (more precisely, RNA/DNA chimera) in real time, thus providing the desired kinetic rate information (Figure 1). Fluorescence-based assays have previously been used to measure the activity of purified RNases in vitro,[5] and fluorescent reporter proteins have been used to indirectly reflect cellular RNA abundance.[6] Our FRET assays are specifically designed to continuously monitor the partitioning between intact and degraded RNA in complex cellular mixtures. In addition, labeling with two fluorophores allows us to test the relative contributions of 5′ to 3′ and 3′ to 5′ exonucleolytic activities to RNA decay.

To study the effects of secondary structure on RNA decay we designed two 16-nucleotide (16 nt) oligonucleotides, RNAs **1** and **2**, that have similar base composition but have two very distinct secondary structures (Figure 1A). Additional design parameters included the incorporation of modified 2′-deoxy thymidines at nucleotide positions 3 and 13 for attachment of fluorescein and tetramethylrhodamine as a donor−acceptor FRET pair.[7] While RNA **1**, under our standard near-physiologic conditions (130 mM potassium glutamate, pH 7.5, 1 mM $MgCl_2$, 10 mM DTT, at 37 °C)[8] is predicted to reside >95% in the stem−loop secondary structure depicted in Figure 1A,[9] RNA **2** is expected to be completely unstructured (Figure 1a). These predictions were confirmed by UV and FRET melting experiments,[10] in which RNA **1** was found to melt at 64 and 61 °C without and with fluorophores attached, respectively, while RNA **2** showed no cooperative melting transition under these conditions.[11] Thus, the attachment of two fluorophores only slightly lowers the melting temperature of RNA **1**, indicating that it only insignificantly interferes with its secondary structure formation.

First, we determined the rate constants for in vitro degradation of RNAs **1** and **2** by RNase T_1 (Figure 1b), which cleaves 3′ to G.[12] RNA decay following addition of 0−250 nM RNase T_1 (pH 7.5) to 50 nM RNA **1** or **2** was monitored as a decrease in steady-state FRET signal (i.e., acceptor:donor fluorescence ratio) under standard conditions, and rate constants k_{dec} were extracted by single-exponential decay fits as described.[7,11] At all [RNase T_1] k_{dec} is greater for the unstructured RNA **2** than for the stem−loop of RNA **1** (Figure 1b). Furthermore, k_{dec} for RNA **1** approaches an asymptotic limit as [RNase T_1] reaches 4-fold excess over the RNA concentration, while k_{dec} for RNA **2** still increases. Fits of cooperative Hill binding equations to the data (Figure 1b) suggest stoichiometric (noncooperative) interaction of the enzyme with both RNAs, with rate constants at saturation of 3.9 min^{-1} for RNA **1** and ≥25 min^{-1} for the unstructured RNA **2** and apparent enzyme affinities K_M of 100 and 330 μM, respectively. Thus, the stem−loop structure of RNA **1** protects it from degradation by RNase T_1 relative to the unstructured RNA **2** (especially given that RNA **1** has more G's, potential RNase T_1 targets, inserted between the fluorophores).

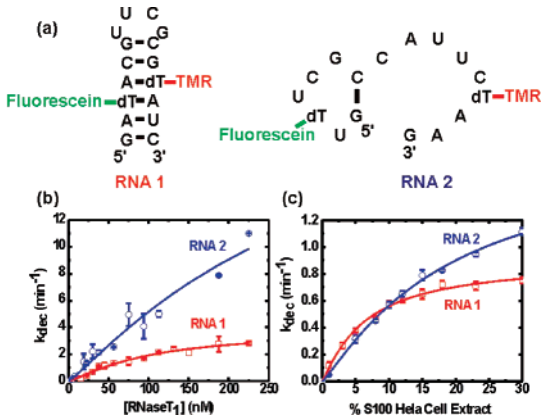

Figure 1. RNA degradation by RNase T_1 and S100 HeLa cell extract as monitored by FRET. (a) RNA folding software was used to predict the secondary structures of RNAs **1** and **2** of this study. The folding free energy of RNA **1** is favorable with −6.0 kcal/mol for a stem−loop structure, while RNA **2** folding is unfavorable at +2.6 kcal/mol.[9] (b,c) Decay rate constants k_{dec} were calculated for degradation of RNAs **1** and **2** by RNase T_1 and S100 HeLa cell extract. Solid lines, fits to the Hill equation.[11]

To show that this kinetic FRET assay also works in complex cellular mixtures, we studied the degradation of RNAs **1** and **2** in S100 cytosolic extract from HeLa cells, a common human epithelial cell line derived from cervix carcinoma. Again, we incubated the RNA under our standard near-physiologic conditions (130 mM potassium glutamate, pH 7.5, 1 mM $MgCl_2$, 10 mM DTT, at 37 °C),[8] then added increasing volume fractions of protease inhibitor treated cell extract (pH 7.6) and analyzed the resultant FRET decrease upon RNA decay as described above.[11] As with RNase T_1, the decay rate constant k_{dec} for RNA **1** approaches an asymptotic limit as the content of cell extract is raised to 30% (v/v), while that of RNA **2** does not (Figure 1c). Fits of the cooperative Hill binding equation to the data indicate noncooperative binding of one RNase enzyme in the cell extract to either RNA (Figure 1c). However, RNA **1** is degraded faster than RNA **2** at <10% (v/v) cell extract, yet slower at >10% (v/v). This results in rate constants at saturation of 0.90 min^{-1} and 1.76 min^{-1} for RNAs **1** and **2**, respectively, and apparent extract affinities of 6.4% (v/v) and 19% (v/v), respectively. Thus, the stem−loop structure of RNA **1** confers some RNase protection, but only at conditions close to the cellular

10.1021/ja036854b CCC: $25.00

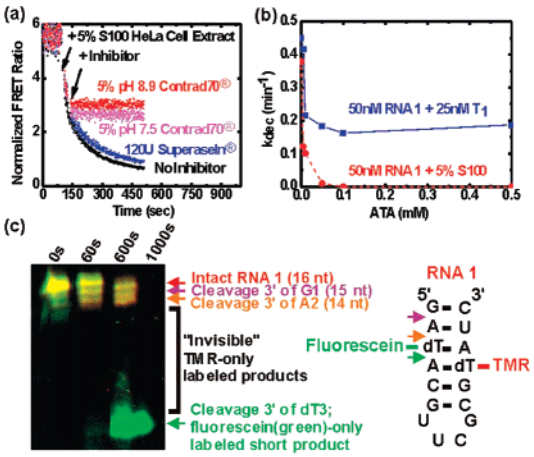

Figure 2. Degradation of 50 nM RNA **1** by 5% (v/v) S100 HeLa cell extract. (a) Contrad70 inhibits degradation by S100 HeLa cell extract, as evident from the lack of a FRET decrease after inhibitor addition, while SuperaseIn has minimal effects. (b) ATA is the most potent inhibitor of RNA **1** degradation by both RNase T_1 and S100 HeLa cell extract. (c) RNA **1** degradation by S100 HeLa cell extract, stopped at the indicated times and analyzed by gelFRET. Primary nuclease activity is that of a 5′ to 3′ exonuclease, as evident from the fluorescein−tetramethylrhodamine-labeled (yellow) 15 nt and 14 nt cleavage bands, followed by a size gap and release of a short fluorescein-only labeled (green) band, as indicated.

environment (highest % (v/v) cell extract). Competition experiments with unlabeled RNA show that the addition of RNA **2** interferes with the degradation of RNA **1** only when added to at least 100-fold excess (5 μM), indicating that the degradative pathways of structured and unstructured short RNAs are at least partially distinct. Similarly, poor competition is observed when adding excess RNA **1** to RNA **2**, suggesting that the observed saturation is due to an intrinsic limit of the decay rate constant, rather than titration of an essential degradative pathway component (data not shown).

To further characterize the utility of our FRET-based RNA decay assays, we tested their ability to report on known and potential RNase inhibitors. Divalent cations, such as Mg^{2+}, inhibit RNase T_1.[13] As expected, addition of increasing [Mg^{2+}] to 50 nM RNA **1** under otherwise standard conditions gradually decreases the rate constant of degradation by 75 nM RNase T_1 from 1.54 min^{-1} at 1 mM Mg^{2+} to 0.73 min^{-1} (that is, by 53%) at 500 mM Mg^{2+}, an effect that is prevented when Mg^{2+} is chelated by EDTA.[11] We also tested other potential inhibitors and found that addition of 10% Contrad70 (Decon Labs, Inc.), a strong, alkaline laboratory detergent, to a final pH of 9.3 inhibits RNase T_1 mediated RNA decay by 97%. Contrad70 at pH 7.5 inhibits by only 30%, consistent with the observation that a pH of 9.3 alone inhibits RNase T_1 already by 74%. Addition of 120 units of SuperaseIn (Ambion), a commercially available RNase T_1 inhibitor, was able to inhibit RNase T_1 by a mere 41%.[11]

To characterize the differences in nucleolytic activity of RNase T_1 and S100 cytosolic HeLa cell extract, the same inhibitors tested on RNase T_1 were added to RNA decay assays of 50 nM RNA **1** by 5% (v/v) cell extract (Figure 2a). Addition of 5% (v/v) Contrad70 inhibits degradation at a final pH of 7.5 and 8.9 by 75 and 97%, respectively (Figure 2a). SuperaseIn (120 units) inhibits cell extract-mediated RNA decay by only 17% (Figure 2a), a substantially smaller extent of inhibition than that observed for RNase T_1. Likewise, up to 500 mM Mg^{2+} does not appreciably inhibit degradation of RNA **1** by cell extract (data not shown), indicating that the major nuclease activity found in S100 cytosolic HeLa cell extract is distinct from RNase T_1 activity. However, in aurin tricarboxylic acid (ATA), a neuroprotective compound and known RNase inhibitor,[14] we found a strong inhibitor of both RNase T_1 and S100 cytosolic HeLa cell extract at pH 7.4 (Figure 2b). We also found it to slightly alter the fluorescence emission profiles of our doubly labeled RNAs, consistent with lower-energy transfer between the donor and acceptor dyes.[11] This suggests that ATA may bind to RNA and alter its secondary structure, thus protecting it from degradation by RNases.

Finally, we utilized inhibition by 10% Contrad70 at pH 9.3 to stop RNase degradation. Reaction products were then analyzed at defined times by 20% denaturing, 7 M urea, polyacrylamide gel electrophoresis, and gelFRET analysis.[15] All possible RNase T_1 cleavage sites were observed for RNA **1**, although cleavage 3′ to G1 and G12 occurred preferentially over cleavage 3′ to G6 and G10 (data not shown). Cleavage at both potential sites was observed for RNA **2**, although cleavage after G1 occurred more rapidly than cleavage after G6 (data not shown), demonstrating a general preference for terminal over internal cleavage sites. Similar experiments using S100 cytosolic HeLa cell extract showed that 5′ to 3′ exonuclease is the predominant RNase activity in the extract for both RNA **1** (Figure 2c) and RNA **2** (data not shown), as is typical for decapped RNA.[1] Degradation was completed by 1000 s, which coincides with our FRET kinetics (Figure 2c).

Here, we have demonstrated the utility of a novel FRET assay to monitor in real-time the degradation kinetics of short RNAs by a purified RNase and in S100 cytosolic HeLa cell extract. We find that single-stranded RNA **2** is degraded more rapidly than the stem−loop RNA **1** under all conditions tested except for low concentrations of cell extract. Furthermore, our assay allows for the observation of in-assay inhibition of the RNase activity using inhibitors such as Contrad70 and ATA. Observation of the exact sites of cleavage using gelFRET confirmed that the change in FRET was a result of nucleolytic activity. Extension of these methods to living cells to probe cellular processes involving short RNAs, such as siRNAs, is under active investigation.

Acknowledgment. This work was supported by NIH Grant GM62357, ACS-PRF Grant 37728-G7, and a Dow Corning endowment. We thank Tom Kerppola for use of his FluorImager, and David Engelke and Danny Reinberg for HeLa cell extract.

Supporting Information Available: Details of RNA synthesis, fluorescence methods, and additional figures (PDF). This material is available free of charge via the Internet at http://pubs.acs.org.

References

(1) (a) Deutscher, M. P.; Li, Z. *Prog. Nucleic Acid Res. Mol. Biol.* **2001**, *66*, 67−105. (b) Hollams, E. M.; Giles, K. M.; Thomson, A. M.; Leedman, P. J. *Neurochem. Res.* **2002**, *27*, 957−980. (c) Tourriere, H.; Chebli, K.; Tazi, J. *Biochimie* **2002**, *84*, 821−837.
(2) Cao, D.; Parker, R. *RNA* **2001**, *7*, 1192−1212.
(3) Hannon, G. J. *Nature* **2002**, *418*, 244−251.
(4) McManus, M. T.; Sharp, P. A. *Nat. Rev. Genet.* **2002**, *3*, 737−747.
(5) Trubetskoy, V. S.; Hagstrom, J. E.; Budker, V. G. *Anal. Biochem.* **2002**, *300*, 22−26.
(6) Chen, C. A.; Cowan, J. A. *Chem. Commun.* **2002**, *3*, 196−197.
(7) (a) Walter, N. G. *Methods* **2001**, *25*, 19−30. (b) Walter, N. G.; Harris, D. A.; Pereira, M. J.; Rueda, D. *Biopolymers* **2002**, *61*, 224−242. (c) Walter, N. G. *Curr. Protocols Nucleic Acid Chem.* **2002**, *11.10*, 11.10.11−11.10.23. (d) Pereira, M. J.; Harris, D. A.; Rueda, D.; Walter, N. G. *Biochemistry* **2002**, *41*, 730−740. (e) Harris, D. A.; Rueda, D.; Walter, N. G. *Biochemistry* **2002**, *41*, 12051−12061. (f) Jeong, S.; Sefcikova, J.; Tinsley, R. A.; Rueda, D.; Walter, N. G. *Biochemistry* **2003**, *42*, 7727−7740.
(8) Christensen, K. A.; Myers, J. T.; Swanson, J. A. *J. Cell Sci.* **2002**, *115*, 599−607.
(9) (a) Mathews, D. H.; Sabina, J.; Zuker, M.; Turner, D. H. *J. Mol. Biol.* **1999**, *288*, 911−940. (b) Zuker, M. *Curr. Opin. Struct. Biol.* **2000**, *10*, 303−310. (c) SantaLucia, J. *Proc. Natl. Acad. Sci. U.S.A.* **1998**, *95*, 1460−1465.
(10) Vamosi, G.; Clegg, R. M. *Biochemistry* **1998**, *37*, 14300−14316.
(11) See Supporting Information.
(12) Deshpande, R. A.; Shankar, V. *Crit. Rev. Microbiol.* **2002**, *28*, 79−122.
(13) Takahashi, K.; Uchida, T.; Egami, F. *Adv. Biophys.* **1970**, *1*, 53−98.
(14) Baba, M.; Schols, D.; Pauwels, R.; Balzarini, J.; De Clercq, E. *Biochem. Biophys. Res. Commun.* **1988**, *155*, 1404−1411.
(15) Ramirez-Carrozzi, V. R.; Kerppola, V. K. *Methods* **2001**, *25*, 31−43.
JA036854B

RNA Degradation in Cell Extracts: Real-Time Monitoring by Fluorescence Resonance Energy Transfer (FRET)

Sarah A. Uhler,† Dawen Cai,† Yunfang Man, Carina Figge, and Nils G. Walter*

Department of Chemistry, University of Michigan, Ann Arbor, Michigan 48109-1055
RECEIVED DATE (automatically inserted by publisher); nwalter@umich.edu

Supporting Information:

RNA Synthesis: All RNA oligonucleotides were obtained commercially from the HHMI Biopolymer/Keck Foundation Biotechnology Resource Laboratory RNA at the Yale University School of Medicine. RNA **1**, the stem-loop RNA, has the sequence GA(dTF)ACGUUCGCG(dTN)AUC where dTF is a fluorescein coupled to a 2'-deoxythymidine and dTN is a 2'-deoxythymidine with a 5' C6-amino linker. The unstructured RNA (RNA **2**) has the sequence GU(dTF)UCGCCAUUC(dTN)AAG, with similar modified bases. RNA oligonucleotides were deprotected and labeled as previously described.[1] The acceptor fluorophore tetramethylrhodamine was post-synthetically coupled to the amino-modifier dTN as described.[1]

Buffer Conditions: A near-physiological standard buffer was prepared containing 130 mM potassium glutamate (introducing ~100 mM K^+) and 1 mM $MgCl_2$ at pH 7.5.[2] DTT was added directly prior to experiments to a final concentration of 10 mM. Since the buffer capacity of glutamate is relatively low around physiological pH, we confirmed that the pH did not change by more than 0.1 pH units upon addition of all supplements to their highest concentration, including RNase T_1 (stored in 50 mM Tris-HCl, pH 7.5, 100 mM NaCl, 0.1 mM EDTA; then diluted in standard buffer to the appropriate concentration), protease inhibitor treated S100 cytosolic extract from HeLa cells (pH 7.6; preparation see below), and acidic aurin tricarboxylic acid (ATA; added to not higher than 0.5 mM final concentration), unless otherwise noted.

S100 Cytosolic Extract From HeLa Cells: This cell extract was a gift from Danny Reinberg (Department of Biochemistry, State University of New Jersey, Rutgers) and was prepared following published protocols.[3] Final step is an extensive dialysis against buffer D, composed of 20 mM HEPES, pH 7.9, 20% (v/v) Glycerol, 100 mM KCl, 0.2 mM EDTA, 0.5 mM DTT, 0.5 mM PMSF; we found the pH after dialysis to be 7.6.

UV Melting Curves: 1 μM unlabeled or doubly fluorophore-labeled RNA was prepared in standard buffer and degassed under vacuum. 260 nm was used as the analytical wavelength for a UV melting experiment, and the signal at 320 nm was subtracted as background. Temperatures ramped up and down from 20 ˚C to 100 ˚C at a rate of 0.2 ˚C/minute using a Beckman DU640B Spectrophotometer with High Performance Temperature Controller and Micro Auto 6 T_m cell holder. Melting temperatures were obtained using MicroCal Origin 7.0 by fitting a Gaussian distribution to the first derivative of the background-corrected 260 nm absorbance vs. temperature plot.

FRET Melting Curves: Fluorescence spectra and intensities were recorded on an Aminco-Bowman Series 2 spectrofluorimeter (Thermo Spectronic). 50 nM double-labeled RNA (200 μL total volume) was prepared in standard buffer, heat-annealed at 70 ˚C for 2 minutes and centrifuge filtered through a 0.45 μm filter. Excitation (500-650 nm) and emission scans (350-570 nm) were collected at 10 nm/s and averaged over 5 repetitions, prior and after the experiment. The cuvette was sealed with Parafilm after carefully inserting a temperature microprobe such that it did not obstruct the light path. Fluorescein was excited at 490 nm (4 nm bandwidth) and fluorescence emission over time was recorded simultaneously at the fluorescein (520 nm, 8 nm bandwidth) and tetramethylrhodamine (585 nm, 8 nm bandwidth) wavelengths for a total of >11,000 sec, by shifting the emission monochromator back and forth. Over the total timeframe, the temperature was ramped from 20 ˚C to 68 ˚C (as measured with the microprobe), at steps of 1-5 ˚C. Once a new temperature became stable for over 100 s after a ramping step, FRET ratios $Q = F_{585}/F_{520}$ were recorded for 100 s (at 1 datum/sec), averaged and normalized to the average FRET ratio at the lowest temperature, Q_0 (i.e., $(Q-Q_0)/Q_0$ was calculated). Corrected FRET ratios were then computed by subtracting the normalized FRET ratios of stem-loop RNA **1** from the corresponding normalized FRET ratios of unstructured RNA **2** to compensate for fluorescence changes not attributed to RNA melting (but rather to direct effects of temperature on the fluorophores). The melting temperature was obtained in MicroCal Origin 7.0 by fitting a Gaussian distribution to the differential of the corrected (and smoothed) FRET ratio vs. temperature plot (Supplemental Figure A).

Steady-state FRET Assays: Steady-state fluorescence spectra and intensities were recorded on an Aminco-Bowman Series 2 spectrofluorimeter, with monochromator settings as above. 50 nM double-labeled RNA substrates were prepared as for FRET melting experiments. Experiments were preformed at 37 ˚C. Excitation (500-650 nm) and emission scans (350-570 nm) were collected at 10 nm/s and averaged over 5 repetitions, prior to kinetic steady-state FRET measurements. RNase T_1 or cell extract was added ~100 s after starting a FRET time course (final volume 200 μL). Mineral oil was then added to prevent sample evaporation. Steady-state measurements were typically collected at 1 datum/sec for 3,000 sec, or longer for slow rate constants, so that the observation window was at least twice the derived time constant τ. The assay conditions (low ionic strength, 37 ˚C) are chosen such that dissociation of most decay fragments will be fast, leading to rapid breakdown of FRET upon cleavage between the fluorescein and tetramethylrhodamine fluorophores. Inhibitor studies using varying concentration of inhibitors were performed by either pre-incubating the sample with inhibitor prior to addition of enzyme, or by adding inhibitors subsequent to addition of enzyme, as indicated. A FRET ratio $Q (= F_{585}/F_{520})$ was calculated and normalized to the initial value Q_0 as above. The resulting time traces were fit to single-exponential decay functions of the form $y = y_o + A_1(1-e^{-t/\tau})$ in MicroCal Origin 7.0 to extract the rate constants $k_{dec} = \tau^{-1}$. To extract Hill parameters, the dependence of the rate constant k_{dec} on a concentration [X] was fit, using MicroCal Origin 7.0, to the Hill equation:[1]

$$k_{dec} = k_{\max} \frac{[X]^n}{[X]^n + K_M{}^n},$$

to yield an apparent affinity K_M for X and a cooperativity or Hill constant n (found to be 1, or non-cooperative).

GelFRET Analysis: GelFRET assays were performed using samples prepared as for steady-state FRET experiments, with 10 pmol FRET labeled RNA per time point. Degradation was arrested at specific times by addition of Contrad70® to a final concentration of 10% (v/v) and a of pH 9.3. Samples were diluted in an equal volume of loading buffer (80% formamide, 0.025% xylene cyanol, 0.025% bromophenol blue, 50 mM EDTA) and loaded onto a denaturing, 20% polyacrylamide, 8 M urea, gel between low-fluorescence glass plates. After electrophoresis for 1 hour at 50 V/cm, the gel was scanned in a FluorImager SI fluorescence scanner with ImageQuant software (Molecular Dynamics) as described previously.[1,4] Briefly, a laser excited fluorescein at 488 nm and the gel was scanned for fluorescence emission using a photomultiplier tube with either a 530 nm band-pass (for the donor fluorescein) or a 610 nm long-pass filter (for the acceptor tetramethylrhodamine). RNAs labeled with only fluorescein and only tetramethylrhodamine were included as color calibration standards. Defining the readout of $F_{\text{fluorescein}}$ as green and $F_{\text{tetramethylrhodamine}}$ as red, the corresponding color images were superimposed using Photoshop 7.0 (Adobe) to generate Figure 2c. A yellow band indicates fluorescence from both fluorescein and tetramethylrhodamine (upon FRET); a green band indicates fluorescein only labeled RNA, while a tetramethylrhodamine only labeled RNA is not detected. Specific cleavage products were identified by comparison with size markers generated by alkaline (cleavage 3' of every nt) and RNase T_1 (cleavage 3' of G) digestion of the same RNA.

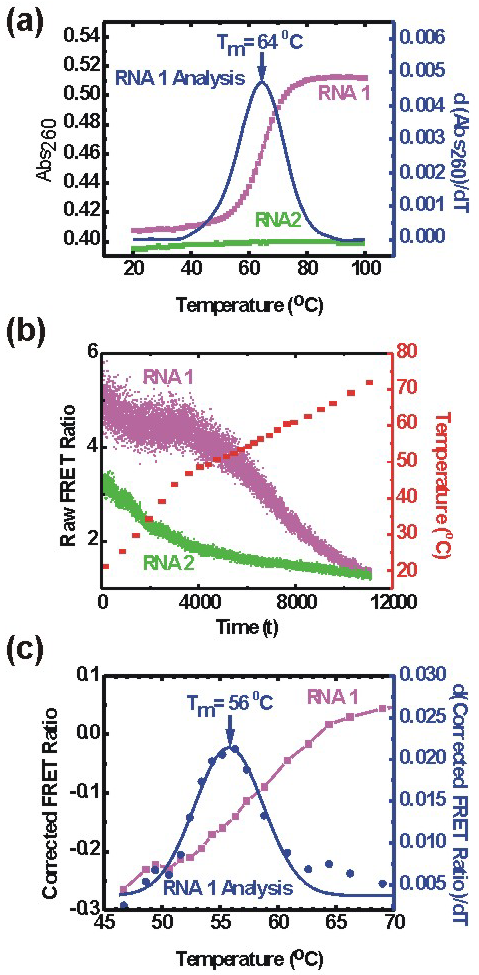

Supplemental Figure A (a) UV melting of RNA to confirm the expected secondary structures of RNAs **1** and **2**. A cooperative melting curve was obtained for RNA **1**, the first derivative of which (blue) fits a Gaussian curve that yields the indicated melting temperature T_m. RNA **2** shows no such melting transition, consistent with its lack of secondary structure. (b) Raw FRET ratios $Q = F_{585}/F_{520}$ of RNAs **1** and **2** upon temperature increase. Over the shown timeframe, the temperature was ramped from 20 ˚C to 68 ˚C, as measured in the cuvette; the red bars indicate time windows in which the given temperature had stabilized. (c) FRET melting curve. In the time windows of stable temperature, FRET ratios were recorded for 100 sec, averaged and normalized to Q at the lowest temperature. Corrected FRET ratios were then calculated by subtracting the normalized FRET ratios of stem-loop RNA **1** from the corresponding normalized FRET ratios of unstructured RNA **2** to compensate for fluorescence changes not due to RNA melting. A Gaussian distribution (blue line) was fit to the first derivative of the corrected and smoothed FRET ratios (blue dots) to yield the indicated melting temperature T_m. The results replicate those of UV melting, demonstrating the ability of FRET to monitor changes in the secondary structure of RNA **1**.

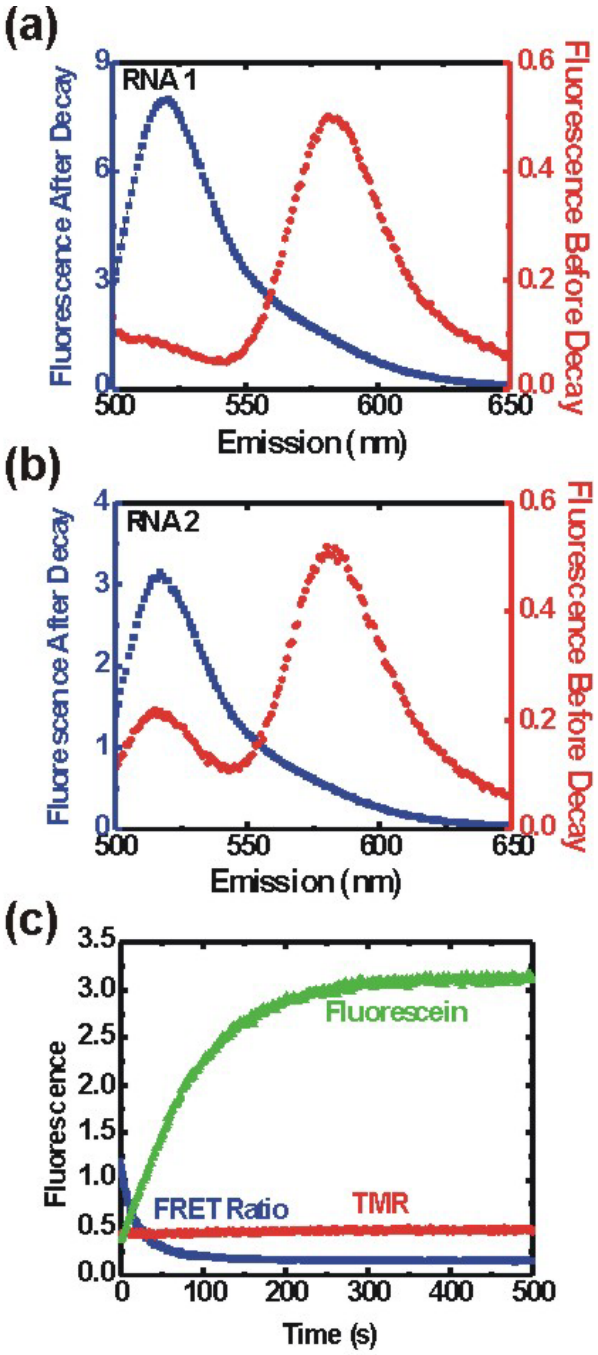

Supplemental Figure B (a) Emission spectrum of 50 nM RNA **1** before and after degradation by 75 nM RNase T_1 in standard buffer at 37 °C. (b) Emission spectrum of 50 nM RNA **2** before and after degradation by 75 nM RNase T_1 in standard buffer at 37 °C. Note that FRET (as indicated by a high 585 nm tetramethylrhodamine peak and a low 520 nm fluorescein peak) in the unstructured RNA **2** is nearly as high as in the stem-loop RNA **1**, and very much higher than in the degraded RNA samples. (c) A typical kinetic steady-state FRET assay records an increase in fluorescein emission and a concomitant decrease in tetramethylrhodamine emission over time due to cleavage of the RNA and breakdown of FRET. Shown here is the degradation of 50 nM RNA **1** by 75 nM RNase T_1 in standard buffer at 37 °C. A rate constant k_{dec} of 1.33 min^{-1} was derived by fitting a single-exponential decay curve to the FRET ratio as described above.

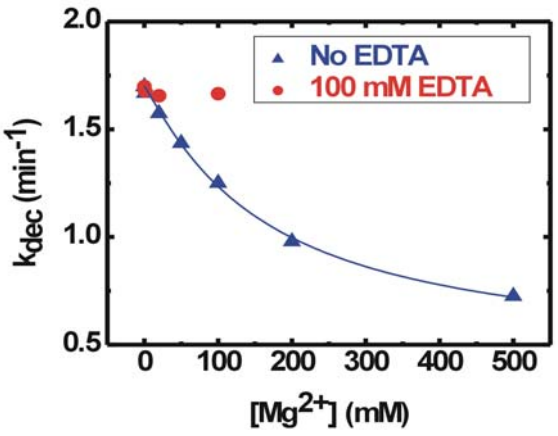

Supplemental Figure C The addition of Mg^{2+} inhibits degradation of 50 nM RNA **1** by 75 nM RNase T_1 in standard buffer at 37 °C. Preincubation with 100 mM EDTA sequesters the Mg^{2+}, thereby preventing the inhibition.

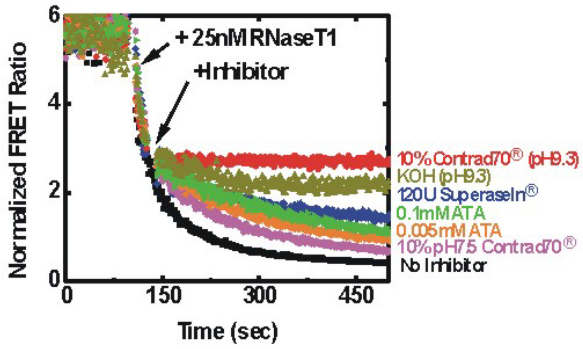

Supplemental Figure D Inhibitor studies using RNase T_1 demonstrate the varying efficacies of Contrad70® at pH 9.3 and 7.5, pH 9.3 alone (adjusted by addition of KOH), SuperaseIn®, and ATA to inhibit degradation of 50 nM RNA **1** by 25 nM RNase T_1 in standard buffer at 37 °C. Inhibition by pH 9.3 alone was reversible, while that by 10% Contrad70 at pH 9.3 was not (data not shown). Rate constants were derived by fitting single-exponential decay curves to the data as described above.

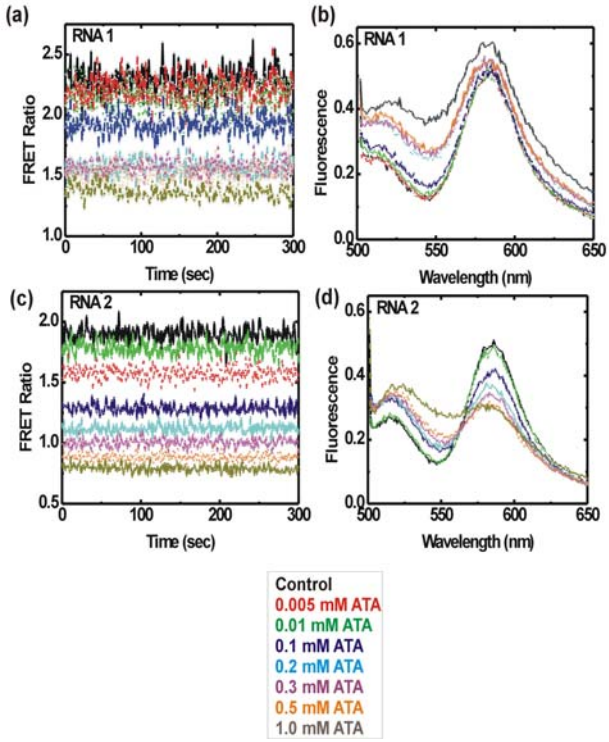

Supplemental Figure E. The RNA structure is modified by the addition of ATA, as monitored by FRET. (a) The FRET ratio for RNA **1** is stable over time but its value depends on the concentration of ATA. (b) The fluorescence emission spectrum of RNA **1** shows an increase in fluorescein emission (peak at 520 nm) in response to ATA addition, while no corresponding increase in tetramethylrhodamine emission (peak at 585 nm) is observed. This indicates either a small change in FRET efficiency or dequenching of fluorescein. (c) The FRET ratio for RNA **2** is stable over time but its value depends on the concentration of ATA. (d) The fluorescence emission spectrum of RNA **2** shows an increase in fluorescein emission (peak at 520 nm) and a corresponding decrease in tetramethylrhodamine emission (peak at 585 nm) in response to ATA addition, a clear indication of a decrease in FRET efficiency. This indicates that the unstructured RNA **2** is affected more by ATA than the stem-loop structure of RNA **1**.

References

(1) (a) Walter, N. G. *Methods* **2001**, *25*, 19-30. (b) Walter, N. G.; Harris, D. A.; Pereira, M. J.; Rueda, D. *Biopolymers* **2002**, *61*, 224-242. (c) Walter, N. G. Curr. *Protocols Nucleic Acid Chem.* **2002**, *11.10*, pp. 11.10.11-11.10.23. (d) Pereira, M. J.; Harris, D. A.; Rueda, D.; Walter, N. G. *Biochemistry* **2002**, *41*, 730-740. (e) Harris, D. A.; Rueda, D.; Walter, N. G. *Biochemistry* **2002**, *41*, 12051-12061. (f) Jeong, S.; Sefcikova, J.; Tinsley, R. A.; Rueda, D.; Walter, N. G. *Biochemistry* **2003**, in press.

(2) Christensen, K. A.; Myers, J. T.; Swanson, J. A. *J. Cell Sci.* **2002**, *115*, 599-607.

(3) Dignam, J. D.; Lebovitz, R. M.; Roeder, R. G. *Nucleic Acids Res.* **1983**, *11*, 1475-1489.

(4) Ramirez-Carrozzi, V.R.; Kerppola, V.K. *Methods* **2001**, *25*, 31-43.